Journal of Photonics for Energy

PhotonicsforEnergy.SPIEDigitalLibrary.org

Pathways toward high-performance perovskite solar cells: review of recent advances in organo-metal halide perovskites for photovoltaic applications

Zhaoning Song
Suneth C. Watthage
Adam B. Phillips
Michael J. Heben

SPIE.

Zhaoning Song, Suneth C. Watthage, Adam B. Phillips, Michael J. Heben, "Pathways toward high-performance perovskite solar cells: review of recent advances in organo-metal halide perovskites for photovoltaic applications," *J. Photon. Energy* **6**(2), 022001 (2016), doi: 10.1117/1.JPE.6.022001.

REVIEW

Pathways toward high-performance perovskite solar cells: review of recent advances in organo-metal halide perovskites for photovoltaic applications

Zhaoning Song, Suneth C. Watthage, Adam B. Phillips, and Michael J. Heben*

University of Toledo, Wright Center for Photovoltaics Innovation and Commercialization, Department of Physics and Astronomy, 2600 Dorr Street, Toledo, Ohio 43606, United States

Abstract. Organo-metal halide perovskite–based solar cells have been the focus of intense research over the past five years, and power conversion efficiencies have rapidly been improved from 3.8 to >21%. This article reviews major advances in perovskite solar cells that have contributed to the recent efficiency enhancements, including the evolution of device architecture, the development of material deposition processes, and the advanced device engineering techniques aiming to improve control over morphology, crystallinity, composition, and the interface properties of the perovskite thin films. The challenges and future directions for perovskite solar cell research and development are also discussed. © *2016 Society of Photo-Optical Instrumentation Engineers (SPIE)* [DOI: 10.1117/1.JPE.6.022001]

Keywords: organo-metal halide perovskites; photovoltaics; advanced engineering; thin film; stability.

Paper 15081SSV received Dec. 30, 2015; accepted for publication Feb. 26, 2016; published online Apr. 15, 2016.

1 Introduction

In 1954, the first practical photovoltaic (PV) device based on crystalline silicon was demonstrated at Bell Laboratories.[1] After many decades of progress, crystalline silicon technology dominates the global PV market with a 55% and 36% market share for polycrystalline- and monocrystalline-silicon modules in 2014, respectively.[2] The remaining 9% of the market was split between a variety of other established and emerging PV technologies, including polycrystalline thin films, amorphous semiconductors, dye-sensitized solar cells (DSSCs), organics, and quantum dot solar cells.[3] To gain market share from crystal silicon solar cells, alternative technologies have to provide a desirable combination of high power conversion efficiency (PCE), low manufacturing costs, and excellent stability. Recent research suggests that organo-metal halide perovskites (OMHPs), with methylammonium lead iodide ($CH_3NH_3PbI_3$ or $MAPbI_3$) being the prototypical example, have the potential to meet these conditions and become competitive in the marketplace. As a result of intensive research efforts across the globe over the past three years,[4–13] perovskite-based solar cell PCEs are now comparable to or better than most other PV technologies, and the simple device processing promises lower manufacturing costs, suggesting the potential to challenge the prevailing silicon technology in the foreseeable future.[14]

The term perovskite refers to the crystal structure of calcium titanate ($CaTiO_3$), which was discovered by the German mineralogist Gustav Rose in 1839 and named in honor of the Russian mineralogist Lev Perovski.[15] In the field of optoelectronics, OMHPs are a group of materials with the formula AMX_3, where A is an organic cation ($CH_3NH_3^+$ or $NH_2CH_3NH_2^+$), M is a divalent metal cation (Pb^{2+} or Sn^{2+}), and X is a monovalent halide anion (I^-, Br^-, or Cl^-). Figure 1 shows the crystal structure and a single crystal of $MAPbI_3$. In a unit cell of the OHMP

*Address all correspondence to: Michael J. Heben, E-mail: michael.heben@utoledo.edu

This review manuscript is also part of the section on "Breakthroughs in Photonics and Energy," highlighting primarily recent advances in the last three years.

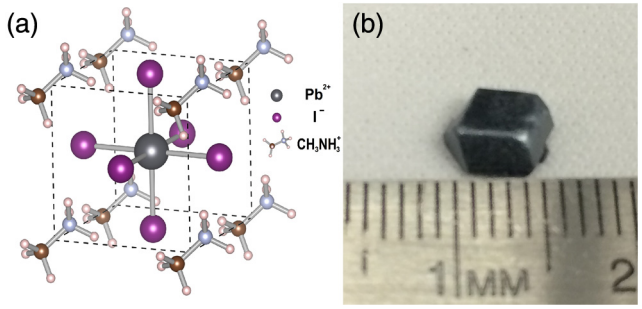

Fig. 1 (a) Crystal structure of $CH_3NH_3PbI_3$ perovskite and (b) photo of a $CH_3NH_3PbI_3$ perovskite single crystal synthesized in our lab using the inverse temperature crystallization method.[16]

structure, eight A^+ cations are located at the vertices of a cubic cage, an M^{2+} cation is located at the center of the cube, and the latter species is octahedrally coordinated to six X^- species that sit at the cube's faces. The OMHP family of materials were studied in the 1990s due to their excellent optoelectronic properties and potential for solution-processed fabrication,[17,18–20] but the main goal of this early work was to develop new materials for field effect transistors and organic light-emitting diodes.[21,22]

The first known use of OMHP was as a dye in DSSC, which reported a 3% PCE in 2009.[23] However, this OMHP-based solar cell contained a liquid electrolyte and received little attention due to the low efficiency and poor stability. The so-called perovskite fever[24] did not fully bloom until a solid-state cell was developed and devices with ~10% efficiency were reported in 2012.[25,26] Since then, OMHP-based PV device performance has rapidly progressed, and a best efficiency record of >21% was achieved in late 2015.[27] The pace of progress has been remarkable and unprecedented in PV history and can likely be attributed to several factors related to inexpensive fabrication costs, ease of processing, and the excellent optoelectronic properties of the materials.[7,9,10–13]

As will be described in Sec. 3, high-quality perovskite thin films can be fabricated using a variety of processes including solution-[26,28] and vapor-based[29–31] deposition methods. Many of these methods are compatible with low-cost, large-scale, industrial production techniques, which strengthens the potential for the commercialization of perovskite solar cells. Due to the ease of processing, many research groups from around the world have been attracted to work in the area. This includes groups that have past histories and relevant expertise in DSSC, organic photovoltaics (OPV), and solution processing. Consequently, the learning curve for developing perovskite solar cells has been relatively short, and progress has been very rapid.

In addition to flexibility in processing, OMHP materials possess several outstanding optoelectronic properties that make them ideal choices for PV applications. The 1.55 eV band gap of $MAPbI_3$ is nearly ideal for single-junction solar cells exposed to the solar irradiance spectrum, and it can be continuously varied in the range from 1.5 to 2.3 eV by exchanging the organic and halide ions.[32,33] The optical absorption coefficient of $MAPbI_3$ is higher than other PV materials such as Si, CdTe, $CuGa_xIn_{1-x}S_ySe_{1-y}$ (CIGS), and amorphous Si:H, so the absorber thickness can be reduced to ~300 nm, thereby lowering the material costs.[34,35] In contrast to organic PV materials, the low exciton binding energy (30 to 50 meV) allows spontaneous exciton dissociation into free charges after light absorption.[36–38] Moreover, the high electron and hole mobility in the range of 10 to 60 $cm^2\ V^{-1}\ s^{-1}$ and the long carrier lifetime (~100 ns) result in long diffusion lengths (~1 μm) so that charge carriers can be freely transported across the 300-nm thick perovskite absorber before recombination.[39–42] Finally, because the electronic defects are shallow and relatively benign, the nonradiative recombination rates are low, allowing open-circuit voltages >1 V to be achieved.[43,44]

Although the perovskite solar cells show great potential, there are several challenges that need to be addressed before commercialization will be possible. Perhaps most significantly, OMHPs have not yet demonstrated the long-term stability that is necessary to compete with the 30-year lifetime of commercially available Si and CdTe solar panels. Second, there are questions about the current–voltage ($J-V$) hysteresis during voltage scanning, which could be problematic for large-scale deployment. There are also concerns associated with potential environmental impacts due to the fact that OMHPs contain Pb.

This review focuses on the recent advances that have allowed perovskite PV to improve to efficiencies >21% in the time period of 2013 to 2015. Reviews that discuss early developments and the materials can be found elsewhere.[7,9,10–13] Here, we provide insights on the key factors that govern the device performance, including device architecture, preparation methods, and advanced device engineering. Notable devices over this time frame are highlighted. Additionally, the stability issues and future directions for perovskite PV devices are discussed.

2 Device Architectures

The first OMHPs employed in PV were used as direct replacements for the dye sensitizers in the DSSCs.[23,45] The typical DSSC structure employs a several-micron thick porous TiO_2 layer that is coated and penetrated with an absorber dye material. The electrode assembly is contacted by a liquid electrolyte containing a redox couple.[46] In these devices, TiO_2 is used to collect and transport the electrons, while the electrolyte acts as a hole conductor. The original perovskite solar cells evolved from this same structure, with the OMHP materials acting simply as a dye replacement.[25,26] Interest increased when the so-called mesoscopic device structure [Fig. 2(a)] was formed by replacing the liquid electrolyte with a solid-state hole conductor.[25,26] This advance created great interest in the PV community and drew in experts from the thin-film PV and OPV communities. As a result, planar device structures in which the OMHP absorber is sandwiched between electron and hole transporting materials (ETM and HTM) were developed. Depending on which transport material is encountered by the light first, these planar structures can be categorized as either the conventional n-i-p [Fig. 2(b)] or the inverted p-i-n [Fig. 2(c)] structures. Recently, a mesoscopic p-i-n structure [Fig. 2(d)] has also been developed.[47,48] Due to processing differences, the device architecture determines the choice of charge transport (ETM and HTM) and collection (cathode and anode) materials, the corresponding material preparation methods, and, consequently, the performance of the devices. To date, no perovskite devices with significant efficiency have been constructed on opaque substrates (e.g., Ti foils)[49,50] because the conventional deposition technologies for transparent conducting oxides (TCO) may lead to decomposition of the surface of the OMHP.

2.1 *Conventional n-i-p Structure*

The mesoscopic n-i-p structure is the original architecture of the perovskite PV devices and is still widely used to fabricate high-performance devices. The structure [Fig. 2(a)] consists of a TCO cathode [fluorine doped tin oxide (FTO)], a 50- to 70-nm thick compact ETM (typically TiO_2), a 150- to 300-nm thick mesoporous metal oxide (mp-TiO_2 or mp-Al_2O_3) that is filled with perovskites, followed by an up to 300-nm perovskite capping layer, a 150- to 200-nm thick layer of 2,2',7,7'-tetrakis(N,N-di-p-methoxyphenylamine)-9,9'-spirobifluorene (spiro-MeOTAD), which is a hole conductor, and 50 to 100 nm of a metal anode (Au or Ag).

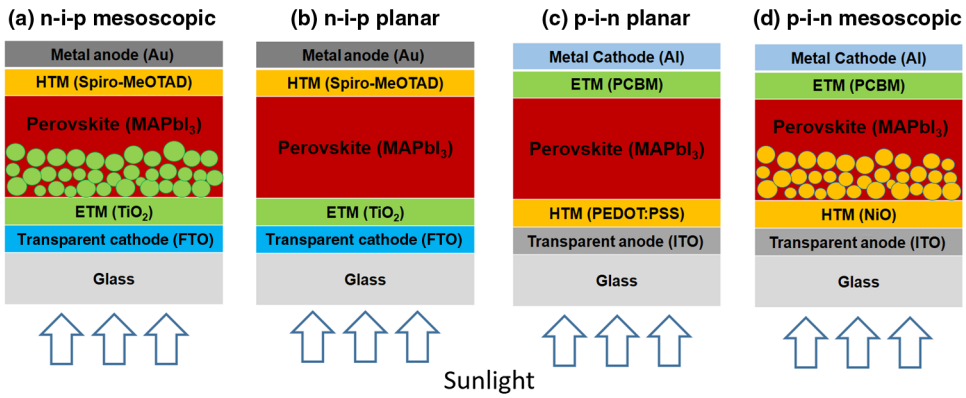

Fig. 2 Schematic diagrams of perovskite solar cells in the (a) n-i-p mesoscopic, (b) n-i-p planar, (c) p-i-n planar, and (d) p-i-n mesoscopic structures.

In this structure, the mesoscopic layer is thought to enhance charge collection by decreasing the carrier transport distance, preventing direct current leakage between the two selective contacts and increasing photon absorption due to light scattering. Accordingly, the original mesoscopic perovskite devices used a thick (>500 nm) porous layer to efficiently absorb the incident light.[25,51] But because the grain growth of the perovskites is confined by the pores in the structure, a significant amount of the material is present in disordered and amorphous phases.[52] This leads to relatively low open-circuit voltage (V_{OC}) and short-circuit current density (J_{SC}).[53] Surprisingly, thinning the mesoporous layer to ~150 to 200 nm results in improved device efficiency due to enhanced crystallinity in the perovskite absorber. Additionally, the pore filling fraction and morphology of the perovskites is critically dependent upon the thickness of mp-TiO_2.[54,55] When the porous layer thickness is reduced to <300 nm, the pore filling fraction is increased and a perovskite capping layer forms on top of the porous structure. Complete pore filling accompanied by formation of a capping layer assures high charge transport rates and high collection efficiencies at the TiO_2 interface. Once the charges are separated, recombination pathways between electrons in the TiO_2 and holes in the HTM are blocked due to the relative positions in energy of the respective conduction and valence bands (*vide infra*).[54] Consequently, the meso n-i-p structure is the most popular structure reported in the literature. The previous record efficiency value (20.2%) was measured from a cell formed in the mesoscopic structure that had discrete perovskite nanocrystals embedded in the porous ETM film with an overlaying continuous and dense perovskite capping layer.[56]

The planar n-i-p structure [Fig. 2(b)] is the natural evolution of the mesoscopic structure. A larger area mesoporous ETM was initially considered critical for high-efficiency perovskite devices because hole extraction at the HTM interfaces is significantly more efficient than electron extraction at the ETM interfaces.[57] However, by delicately controlling the formation of the perovskite absorber, and the interfaces among the perovskite, carrier transport layers, and electrodes, high efficiencies can now be achieved without a mesoporous layer.[58] To date, the best planar n-i-p device showed a 19.3% efficiency after careful optimization of the electron selective indium tin oxide (ITO)/TiO_2 interfaces.[58] Although the planar n-i-p perovskite solar cell usually exhibits enhanced V_{OC} and J_{SC} relative to a comparative mesoscopic device processed with the same materials and approach, the planar device usually exhibits more severe $J-V$ hysteresis (see Sec. 6). Thus, the state-of-the-art n-i-p devices usually include a thin (~150 nm) mesoporous buffer layer filled and capped with the perovskite.[56]

2.2 *Inverted p-i-n Structure*

When the deposition order is changed and the HTM layer is deposited first, the device is fabricated in the p-i-n structure [Fig. 2(c)]. In this case, the p-i-n type perovskite device is built on a 50- to 80-nm p-type conducting polymer such as poly(3,4-ethylenedioxythiophene) poly(styrene-sulfonate) (PEDOT:PSS), which is deposited on ITO-coated substrates. After depositing a 300-nm intrinsic perovskite thin film, the device is completed with a 10- to 60-nm organic hole-blocking layer [6,6]-phenyl C_{61}-butyric acid methyl ester (PCBM) and a metal cathode (Al or Au). Early device design utilized a perovskite and fullerene (C_{60}) donor–acceptor pair, which is typical in OPV.[59] In fact, the commonality in structure has allowed OPV researchers to easily move into the field of perovskites. As the field has advanced, the organic acceptor has been omitted in favor of an ETM layer, leaving the planar perovskite absorber sandwiched between two opposite organic charge transporting materials.[60] Recently, the efficiency of the planar p-i-n device has improved significantly due to the use of more advanced material preparation methods, such as a multicycle solution coating process, and a best efficiency of 18.9% was achieved.[61]

Further development of the p-i-n device structure has expanded the selective contact options from organic to inorganic materials. For example, NiO and ZnO/TiO_2 layers have recently been used for the hole and electron selective contacts, respectively, which makes the perovskite device distinct from its organic conterpart.[62,63] Inorganic charge extraction layers (NiMgLiO and $TiNbO_2$) have been used to fabricate large-area (1 cm^2), high-efficiency (15%) perovskite cells, representing a potentially important step in the path toward commercialization.[62] The use of oxide HTMs also allows for construction of the mesoscopic p-i-n device structure [Fig. 2(d)],

in which NiO/mp-Al_2O_3 or c-NiO/mp-NiO are used as the HTM.[47,48] The best mesoscopic p-i-n device with a nanostructured NiO film demonstrated a 17.3% efficiency.[64]

3 Preparation Methods

The device performance of most thin-film solar cells is mainly determined by the film quality of the absorber. High-quality perovskite films with appropriate morphology, uniformity, phase purity, and crystallinity are essential for high-performance PV devices. To meet these quality criteria, well-controlled crystallization and engineering of the composition and interface properties of perovskite films are required. Critical issues include the deposition approach, precursor composition, processing condition, and additive control, all of which can greatly affect the crystallization and quality of the perovskite films. Focusing first on the deposition approach, the preparation processes can be categorized as follows: single-step solution deposition,[26] two-step solution deposition,[28] two-step vapor-assisted deposition,[30] and thermal vapor deposition.[29]

3.1 *Single-Step Solution Deposition*

Single-step solution deposition [Fig. 3(a)] is commonly used for perovskite thin film preparation due to ease of processing and low fabrication cost. Generally, organic halides [methylammonium iodide (MAI)] and lead halides (PbX_2, X = I, Br, or Cl) are dissolved in gamma-butyrolactone (GBL), dimethylformamide (DMF), or dimethyl sulfoxide (DMSO) to prepare the precursor solution. The perovskite films can be prepared by spin-coating of the precursor solution followed by a postdeposition heating at 100 to 150°C. Since the perovskite tolerates composition variation,[65] high-efficiency devices can be fabricated through a wide range of MAI to PbI_2 precursor ratios from MAI-poor (1:2)[66] to MAI-rich (3:1).[58] However, it is critical to choose appropriate processing temperatures and times based on differing precursor compositions to achieve the desired crystallinity, phase, and morphology of the perovskite films.[55,65,67] In addition to the choice of precursor composition and processing temperature, the environment (oxygen and humidity levels), substrate material, and deposition parameters must also be controlled. The first solid-state device prepared using the single-step solution process produced a perovskite device that exhibited 9.7% efficiency.[68] After developing advanced engineering techniques (discussed in Sec. 4), a best efficiency of 19.7% has been achieved with single-step solution deposition.[69]

In addition to spin-coating, other solution-based deposition methods, including spray,[70] doctor-blade,[71] inkjet printing,[72] and slot-die printing,[73] have also been employed to fabricate perovskite PV devices. These techniques demonstrate the potential for large-scale roll-to-roll manufacture of perovskite solar cells. However, the efficiency of devices prepared by these methods is still lower than that of spin-coated devices due to the difficulties associated with controlling the film morphology and compositional uniformity at present.

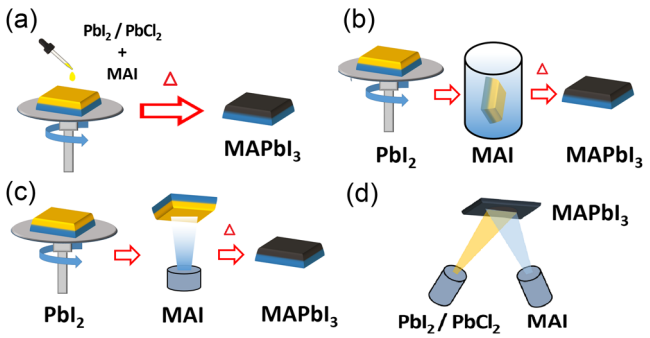

Fig. 3 Deposition methods for perovskite thin films, including (a) single-step solution deposition, (b) two-step solution deposition, (c) two-step hybrid deposition, and (d) thermal vapor deposition.

3.2 *Two-Step Solution Deposition*

The two-step solution deposition approach to preparing OMHPs was first introduced by Mitzi et al. in 1998.[74] Following this pioneering work, Gratzel et al. developed a sequential deposition method [Fig. 3(b)] to prepare perovskite solar cells, which has resulted in efficiencies >15%.[28] In a typical two-step solution procedure, a PbI_2 seed layer is spin-coated and then converted to $MAPbI_3$ by dipping the substrate into an MAI/isopropanol solution.[28] Spin-coating has also been used to introduce MAI molecules into the PbI_2 network.[68] Compared with the single-step solution process, the two-step sequential deposition process results in more uniform and dense perovskite films.[75] The process can be well controlled and, consequently, has been extensively used to fabricate high-efficiency devices.[28,56,76,77]

The two-step solution method provides a reproducible way to fabricate high-quality perovskite thin films. Through varying the MAI solution concentration, the perovskite grain size can be controlled.[68] However, one of the drawbacks of the two-step solution deposition method is the trade-off between perovskite grain size and surface smoothness. Films with large perovskite grains typically exhibit poor surface coverage, which can limit the performance of devices. The other issue with this method is incomplete perovskite conversion. The conversion from PbI_2 to $MAPbI_3$ rapidly occurs as the film is dipped into the solution because the layered structure of heavy metal halide is prone to interaction with small molecules.[78] Thus, a dense perovskite capping layer usually forms on the surface of PbI_2 and hinders the MAI diffusion to the underlying layer, leading to incomplete perovskite conversion. These issues have been overcome by some new techniques that have been developed recently (Sec. 4), and now the champion cell efficiency using the two-step solution method has been improved to 20.2%.[56]

3.3 *Vapor-Assisted Solution Deposition*

In one modification to the two-step solution deposition method, MAI is introduced through a vapor deposition technique rather than through solution processing [Fig. 3(c)].[30] This deposition method allows better control of morphology and grain size via gas–solid crystallization and effectively avoids film delamination that can occur during liquid–solid interaction. The perovskite films prepared by this method exhibit uniform surface coverage, large grain size, and full conversion. However, the use of this method is limited because the gas–solid reaction typically required tens of hours for the full conversion, and devices prepared by this method have exhibited only 10 to 12% efficiency.[30,79]

3.4 *Thermal Vapor Deposition*

Vapor phase deposition is widely used for fabricating high-quality semiconductor thin films with uniform thickness and composition. The thermal vapor deposition of OMHP thin films was first demonstrated by Mitzi et al. in 1999.[18] After modifying the technique for dual-source thermal evaporation [Fig. 3(d)], Snaith et al. prepared the first planar heterojunction $MAPbI_{3-x}Cl_x$ perovskite solar cell with an efficiency that exceeded 15%.[29] Similar vapor-based deposition techniques, such as sequential layer-by-layer vacuum sublimation[31] and chemical vapor deposition,[80] have also been developed.

The perovskite films prepared by thermal vapor deposition are extremely uniform and pinhole-free. Compared with the incomplete surface coverage that can be found for perovskite films prepared by solution processing, vapor-deposited perovskite layers can conformally coat TiO_2 and PEDOT:PSS layers.[29,60,81] However, both the precursor sources and the products have low thermal stability, so the vapor deposition requires precise control over temperatures during deposition. Thus, only a few research groups have reported high-efficiency devices prepared by this method.[29,31,60,81,82]

4 Advanced Device Engineering

In early 2013, the state-of-the-art of perovskite solar cells prepared by various deposition techniques had demonstrated device efficiencies in the range of 12 to 15%.[28–30] Since then,

the efficiency has improved to 18 to 20%, mainly due to the advancements of several device engineering strategies.[10,83,84] These engineering strategies, which focused on controlling the precursor solution, processing condition, perovskite composition, and interface properties, lead to smooth and pinhole-free perovskite thin films consisting of large grains with good crystallinity. The combination of these advanced engineering methods has improved the optoelectronic properties of the perovskite films and, consequently, the device performance as well.

4.1 *Solvent Engineering*

Single-step spin-coating is the simplest method for preparing perovskite thin films; however, it is difficult to achieve a homogeneous composition and uniform thickness over large areas. The reason for this is that single-step solution deposition using DMF and GBL solvents often results in the formation of needle- and spherical-shaped colloidal intermediates.[28,85] To improve the surface morphology of spin-coated perovskite films, several precursor solution additives have been employed to suppress the formation of deleterious intermediates.

DMSO is one of the best and widely used additives.[77,86] The precursor solution with added DMSO forms a uniform and flat MAI-PbI_2-DMSO intermediate film when spin-coated. After a thermal treatment, the intermediate film is converted into a uniform perovskite film through a solid-state reaction. Several other additives, such as CH_3NH_3Cl,[87] HI,[88] I_2,[89] NH_4Cl,[90] H_2O/HBr,[91] 1,8-diiodooctane,[92] aminovaleric acid,[93] and phosphonic acid ammonium,[94] have also been used to improve the crystallinity and morphological uniformity of perovskite films.

The formation of uniform perovskite film by incorporating additives is the result of decoupling the nucleation and grain growth processes. For precursor solutions without additives, these two processes occur simultaneously. Since grain growth favors large-size nuclei (the free energy of volume expansion eclipses that of interface formation), the unbalanced growth rate leads to the formation of large perovskite grains with a significant number of voids between grains. The introduction of additives retards the crystallization kinetics of perovskite formation and results in a uniform intermediate phase film during deposition. A thermal treatment provides the energy for conversion to the perovskite phase and promotes crystal growth to form pinhole-free films.

Additive incorporation was introduced to the two-step methods after its success in single-step deposition. The precursor solution for PbI_2 can be mixed with DMSO,[95] H_2O,[96] and low concentrations of MAI[76] to improve the surface coverage of the final perovskite film. As with single-step deposition, the introduction of additives results in an intermediate state that retards the rapid reaction between MAI and PbI_2 and effectively avoids the formation of a dense perovskite capping layer on the surface of the PbI_2 layer that hinders further conversion.

4.2 *Process Engineering*

In addition to modifying the precursor solution, improved device performance has been achieved by adapting the deposition and postdeposition processes. While slowing the crystal growth kinetics has resulted in higher-quality films, the same results have been obtained by speeding the nucleation kinetics. Hot casting, in which crystallization of the perovskite film occurs immediately after a hot precursor solution is loaded onto the substrate at an elevated temperature, has been used to obtain pinhole-free perovskite films with millimeter-scale grains.[97] Using this approach, the island-shaped grains rapidly integrate into a dense perovskite film with millimeter-size grains following Volmer-Weber growth.[98] Devices with efficiency of ~18% were fabricated using this technique.[97]

Another demonstration of process engineering for fabricating extremely uniform and dense perovskite films is adding an antisolvent that does not dissolve perovskite films (e.g., toluene) during the last few seconds of the spin process.[77] The introduction of toluene rapidly extracts DMF from the precursor solution, which results in a rapid precipitation of perovskite before significant growth of the perovskite grains. Thus, a dense, small-grain perovskite film can form uniformly across the entire substrate surface. In addition to toluene, other antisolvents, such as diethyl ether,[69] chlorobenzene, benzene, and xylene, are also effective in forming highly uniform perovskite films.[99] Since the grain growth kinetics are suppressed during the deposition,

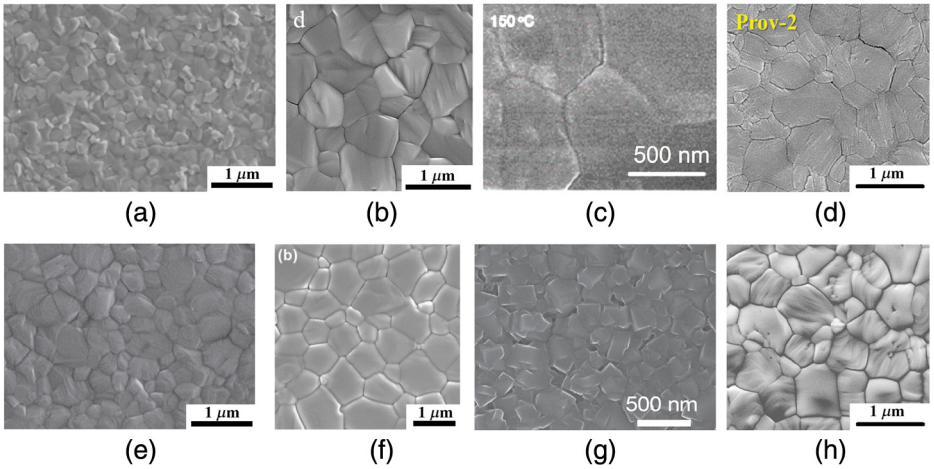

Fig. 4 SEM images of perovskite films prepared using various deposition techniques and advanced engineering processes, including (a) vapor deposition, (b) vapor-assisted deposition, (c) hot casting, (d) H_2O additive, (e) DMSO + toluene, (f) chlorobenzene, (g) sequential deposition, and (h) solvent annealing. Reprinted with permission from Refs. 29, 30, 98, 96, 77, 99, 68, and 100.

this process needs an optimized thermal annealing to achieve both smooth morphology and large grain size.

The postdeposition grain growth process can also be engineered to achieve a uniform and high-quality perovskite film. Although thermal annealing helps increase grain size and improve crystallinity, it may cause decomposition of the perovskite phase and reduce surface coverage.[55,65] Solvent annealing with DMF leads to recrystallization and regrowth of perovskite grains, resulting in improved crystallinity and electronic properties and enhanced device efficiency (15.6%).[100] Annealing with pyridine or MAI vapor has demonstrated enhanced luminescence and carrier lifetimes, indicating the formation of high-quality absorber material and the potential for high-efficiency devices.[101,102]

The advanced solvent and process engineering techniques both aim to decouple the nucleation and growth processes so that the perovskite film formation can be precisely controlled. By applying one or a combination of these techniques, high-quality perovskite films with smooth morphology and large grains were prepared (Fig. 4) and devices with efficiencies of 15 to 19% were fabricated. Details on these devices are summarized in Table 1.

4.3 *Band Gap Engineering*

The tunability of the OMHP band gap over a wide range of the solar spectrum has led to considerable improvement in device performance. Compositional engineering of $MAPbI_3$ perovskite can be achieved by exchanging the organic [formamidinium (FA)], metal (Sn), or halide (Br or Cl) ions. The band gap of the perovskite can be controllably tuned to cover almost the entire visible spectrum from 1.5 to 2.3 eV by introducing mixed halides (I and Br).[32,33] The introduction of Br also enhances the water resistance of the perovskites.[32] Partial replacement of MA by FA for the alloyed $MA_xFA_{1-x}PbI_3$ is an effective way to extend the absorption to longer wavelengths and enhance the thermal stability.[108] With the $(FAPbI_3)_{1-x}(MAPbBr_3)_x$ absorber, solar cells with over 19% average efficiency have been fabricated with a high degree of reproducibility.[56]

In addition to varying the halide anions and the organic cations, the divalent metal cation may also be changed. Due to concerns about lead toxicity, lead-free perovskites, such as $MASnX_3$, have attracted increasing attention.[109–111] Comparing with the Pb-based perovskite, the relatively lower band gap of $MASnI_3$ (~1.3 eV) allows absorption over a broader range and an increase of J_{SC} from 15 to 21 mA/cm^2.[112] The efficiency (~6%) and stability of the lead-free perovskite-based device, though, are not currently comparable to their Pb-based counterparts at this time.

Table 1 Summary of notable perovskite devices.

Year	V_{OC} (V)	J_{SC} (mA/cm^2)	FF (%)	PCE (%)	Device structure	Method	Advanced device engineering	Ref.
2012	0.89	17.6	62	9.7	FTO/c-TiO_2/mp-TiO_2/$MAPbI_3$/spiro/Au	SSS	—	25
2012	0.98	17.8	63	10.9	FTO/c-TiO_2/mp-Al_2O_3/$MAPbI_{3-x}Cl_x$/spiro/Au	SSS	Al_2O_3[(c)]	26
2013	0.99	20.0	73	15.0	FTO/c-TiO_2/mp-TiO_2/$MAPbI_3$/spiro/Au	TSS	—	28
2013	1.07	21.5	67	15.4	FTO/c-TiO_2/$MAPbI_{3-x}Cl_x$/spiro/Au	TVD	—	29
2013	0.92	19.8	66	12.1	FTO/c-TiO_2/$MAPbI_3$/spiro/Au	VAS	—	30
2014	0.94	23.3	65	14.2	FTO/c-TiO_2/$FAPbI_3$/spiro/Au	SSS	FA[(b)]	33
2014	0.84	21.1	65	11.6	FTO/c-TiO_2/mp – TiO_2/ZrO_2 – $MAPbI_3$/C	SSS	ZrO_2[(c)]	93
2014	1.11	19.6	76	16.5	FTO/c-TiO_2/mp – TiO_2/$MAPbI_{3-x}Br_x$/PTAA/Au	TSS	DMSO[(a)], toluene[(p)]	77
2014	1.13	22.8	75	19.3	ITO-PEIE/γ-TiO_2/$MAPbI_{3-x}Cl_x$/spiro/Au	SSS	Polyethyleneimine ethoxylated (PEIE)[(c)], γ-TiO_2[(c)]	58
2014	0.92	22.4	82	17.7	FTO/PEDOT:PSS/$MAPbI_{3-x}Cl_x$/PCBM/Al	SSS	Hot-casting[(p)]	97
2015	1.08	22	73	19	FTO/c-TiO_2/mp-TiO_2/$FA_xMA_{1-x}PbBr_yI_{1-y}$/PTAA/Au	SSS	DMSO[(a)], toluene[(p)], FA and Br[(b)]	103
2015	1.10	20.9	79	18.1	ITO/PEDOT:PSS/$MAPbI_3$/PCBM/Au	SSS	HI[(a)]	104
2015	1.10	22	78	18.9	ITO/PTAA/$MAPbI_{3-x}Cl_x$/PCBM/C60/BCP/Al	SSS	Multicycle[(p)]	61
2015	1.06	24.7	78	20.2	FTO/c-TiO_2/mp – TiO_2/$FA_xMA_{1-x}PbBr_yI_{1-y}$/PTAA/Au	TSS	DMSO[(a)], FA and Br[(b)]	56
2015	1.14	21.3	74	18.4	FTO/SnO_2/$FA_xMA_{1-x}PbBr_yI_{1-y}$/spiro/Au	SSS	DMSO[(a)], FA and Br[(b)], SnO_2[(c)] chlorobenzene[(p)]	105
2015	1.09	22.4	80	19.1	FTO/c-TiO_2/mp-TiO_2/$MAPbI_3$/spiro/Au	SSS	PbI_2[(a)]	66
2015	1.09	23.8	76	19.7	FTO/c-TiO_2/mp – TiO_2//$MAPbI_3$/spiro/Ag	SSS	DMSO[(a)], diethyl ether[(p)]	69
2015	1.08	23.9	75	19.4	FTO/c-TiO_2/$MAPbI_3$/spiro/Au	SSS	Chlorobenzene[(p)]	106
2015	1.05	22.2	76	17.7	ITO/Cu:NiO_x/$MAPbI_3$/C60/Ag	SSS	Toluene[(p)], Cu:NiO_x[(c)]	107
2015	1.07	20.6	75	16.2	FTO/NiMgLiO/$MAPbI_3$/PCBM/Ti(Nb)O_x/Ag	SSS	DMSO[(a)], NiMgLiO[(c)], Ti(Nb)O[(c)]	62

Note: SSS, single-step solution; TSS, two-step solution; TVD, thermal vapor deposition; VAS, vapor-assisted solution. Labels for advanced device engineering techniques: additive (a), processing (p), band gap (b), and contact (c).

4.4 *Contact Engineering*

In addition to controlling and modifying the optoelectronic and structural properties of the absorber, as discussed above, the properties of the electron and hole collecting electrodes and their interfaces are also critical for improving perovskite device performance. The importance of the interface properties has been revealed by electron-beam–induced current investigations, which show that efficient charge separation and collection occur at the interfaces between the perovskite and both charge-selective layers.[113] The choice of the ETM and HTM is important to achieve a high degree of charge selectivity while maintaining a low surface recombination to minimize energy loss at the heterojunction interfaces. Recently, a variety of ETMs and HTMs have been explored for achieving high-efficiency perovskite devices. Figure 5 plots the energy levels for several representative components of the most common perovskite solar cells.

Metal oxides are the most common ETMs. While TiO_2 is predominant in the literature, many other materials can operate as either mesoporous or planar ETMs. Wide band gap metal oxides, such as ZnO,[114] Al_2O_3,[26,115] $SrTiO_3$,[116] SiO_2, and ZrO_2,[93,117] have been used to fabricate devices in the mesoscopic structure. An electrically insulating mesoporous layer allows high V_{OC} to be achieved if there is a lack of sub-band gap and surface electronic states.[26] A variety of ETMs have also been used to form compact layers in the planar n-i-p structure, including ZnO,[118] SnO_2, [105,119] CdSe,[120] CdS,[121] and TiO_2-graphene.[122] Among them, SnO_2 has been used to fabricate an 18% efficiency device, presumably due to good band alignment.[105]

The commonly used HTMs fall into three categories: small molecules, organic polymers, and inorganics. Small molecules, especially spiro-MeOTAD, are very commonly used as the HTM in high-efficiency perovskite PV devices. The conductive organic polymer poly(triarylamine) (PTAA) has recently emerged as a strong competitor to spiro-MeOTAD and was employed in the 20.2% efficiency perovskite device.[56] Poly(3-hexylthiophene-2,5-diyl) and other organic molecules and polymers have also been used to fabricate 12 to 15% efficiency perovskite devices. A detailed review of HTMs can be found elsewhere.[123] Organic HTMs are typically doped with lithiumbis(trifluoromethanesulfonyl)imide and 4-tertbutylpyridine to improve hole conductivity, doping uniformity, and device performance. Although these organic HTMs provide good carrier transport properties, which lead to high performance, high materials costs and unproven long-term stability are major impediments to industrial application. In contrast, inorganic HTMs, such as CuSCN,[124,125] CuI,[126] NiO,[127] and $Cu:NiO_x$,[107] are promising for more cost-effective and stable performance. The highest efficiency reported to date for an inorganic material was 17.7% with $Cu:NiO_x$ as the HTM.[107]

It should be noted that HTM-free and ETM-free designs have also attracted attention. The HTM is not a prerequisite for perovskite solar cells when a high-quality perovskite layer with benign interface properties is presented. A high work function metal (Au or C) may help to extract holes from the perovskite absorber alone. Several groups have demonstrated

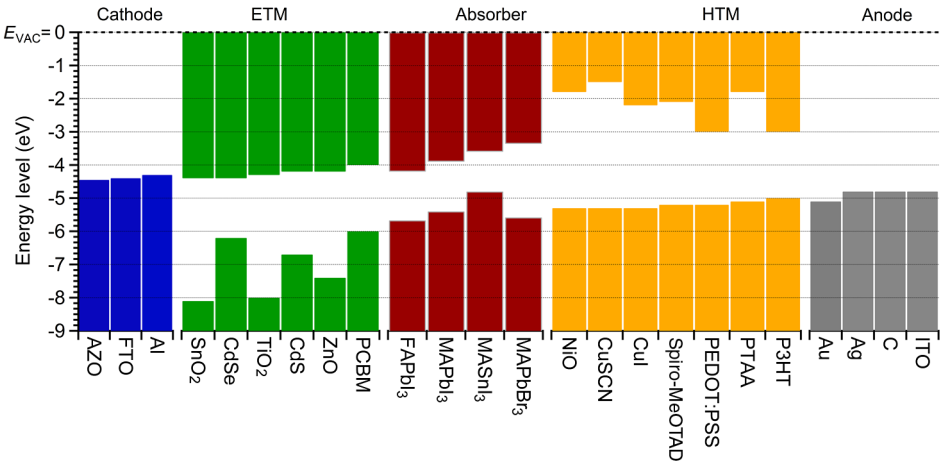

Fig. 5 Diagram showing the energy levels, from left to right, for representative cathode, n-type (ETM), absorber, p-type (HTM), and anode materials.

HTM-free perovskite solar cells with efficiencies ranging from 5 to 12%.[79,93,128–130] In addition to HTM-free devices, ETM-free devices with efficiencies of ~14% have been reported.[131,132] In these devices, the interface properties of the TCO cathode were modified, and the perovskite solar cells were grown directly on FTO substrates without an ETM layer. Although the performance of these devices is inferior to state-of-the-art perovskite devices due to a poor charge extraction and undesired surface recombination at the interface, the designs help improve the understanding of the device physics.

5 Notable Devices

By combining a variety of advanced techniques, several research groups have achieved high-performance perovskite PV devices with efficiencies >17% during the last two years. Over the past three years, the device performance has improved from 10%. Several notable perovskite devices reported in recent years are summarized in Table 1. Figure 6 shows a map of the critical device performance metrics. It is clear that the evolution of the state-of-the-art perovskite device efficiency was achieved by the enhancements in J_{SC}, V_{OC}, and fill factor (FF). Improvements in the 2012 to 2013 timeframe can be attributed to the developments of absorber preparation techniques that led to better morphology and surface coverage and contact engineering techniques that promised efficient charge separation and collection, and, consequently, higher photogenerated current density (Fig. 6). The device efficiency over this time frame was improved from 10 to ~15% by optimizing the basic processing of the perovskite absorber.

All high-performance perovskite devices share some common characteristics. First, a high J_{SC} is typically the result of a dense and uniform perovskite film with appropriate thickness, good crystallinity, and large grain size. The high V_{OC} is enabled by reducing intergrain and intragrain defect densities and by good interface properties between the perovskite and the selective charge collectors. FFs are typically very high, with many devices having FFs in the range of 0.75 to 0.80. Additionally, compositional engineering of the perovskite absorber contributes to better device performance. Incorporating FA extends the absorption range to wavelengths longer than 800 nm, hence enhancing the J_{SC} by ~4 mA/cm^2. The introduction of Br, on the other hand, increases the bang gap of the perovskites and reduces defect density, thus improving the V_{OC} to ~1.1 V.

The highest-efficiency devices typically employ a combination of several advanced engineering techniques. For instance, the champion 20.2% device was prepared by the intermolecular exchange process involving the reaction between the PbI_2-DMSO intermediate phases and the FAI-MABr contained solution.[56] An extremely uniform and dense perovskite film was formed after annealing, and the device exhibited excellent performance (Fig. 7). Other devices with >18% efficiency are fabricated by spin-coating of the mixed PbI_2-FAI-$PbBr_2$-MABr precursor in the DMF/DMSO solution followed by antisolvent quenching.[69,103,105]

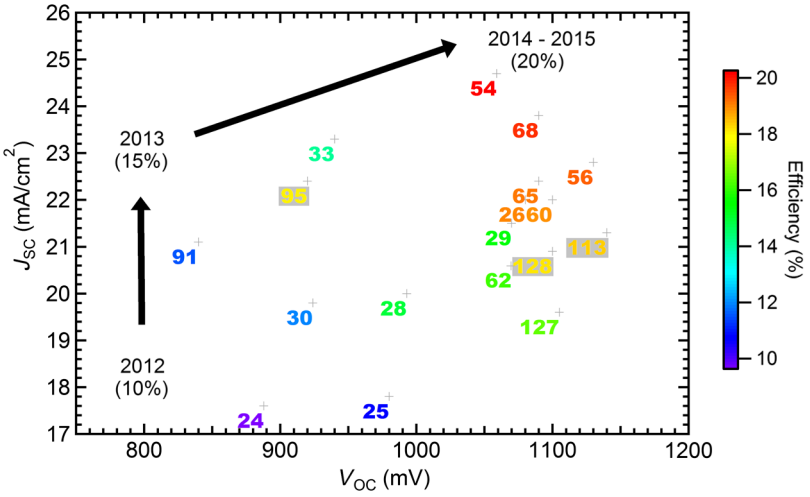

Fig. 6 Efficiency mapping of recently reported state-of-the-art perovskite solar cells labeled with reference number and colored based on efficiency.

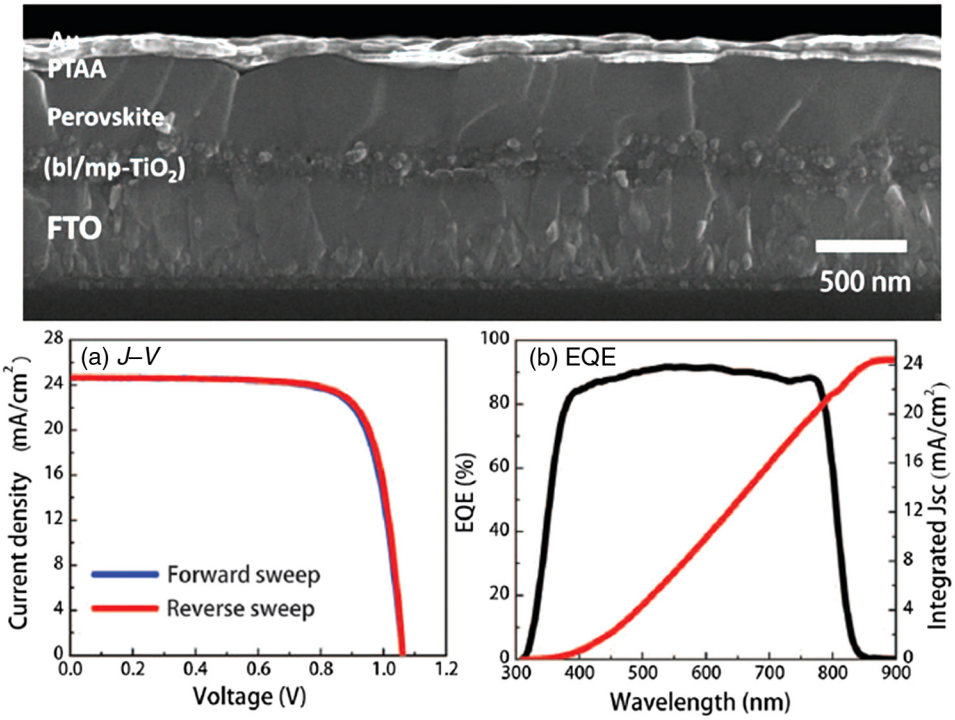

Fig. 7 SEM cross-sectional image and the (a) $J - V$ and (b) external quantum efficiency characteristics of the best-efficiency perovskite PV devices so far. Reprinted with permission from Ref. 56.

6 Issues and Challenges

Perovskite solar cells have demonstrated high efficiency and are being investigated as a viable commercial option. However, the crucial issues and challenges that limited the commercialization of perovskite-based PV remain. Long-term device stability during operation under stressed conditions (high humidity, elevated temperature, and intense illumination) has yet to be demonstrated. The existence of the $J - V$ hysteresis limits the standardized characterization of device performance. Environmental impacts during the manufacturing, operational, and disposal phases of perovskite solar cells are unclear, leaving concerns about the toxicity and contamination associated with the water-soluble lead compounds. Although the complexity of the diverse material preparation methods and device architectures make it more difficult to address these issues, recent progress has provided insights into these issues and the corresponding material properties.

6.1 *Device Stability*

One of the most important criteria for a practical solar cell is that the cell has to maintain a stable power output under a standard working condition. At present, the efficiency of perovskite devices is determined by the average of the forward and reverse scans or the steady-state power output close to the maximum power point. Although $J - V$ hysteresis may exist, the current output of most perovskite devices quickly stabilizes at the maximum power point. Such steady-state output shows the potential for sustainable power generation and is now accepted as one of the criteria to characterize perovskite PV devices.[133]

Although stability data up to a few hundred hours (one to four months) has been reported,[25,93,133] long-term stability that is comparable to the 30-year standard of commercial PV panels has yet to be demonstrated. Early perovskite devices without encapsulation have shown stable operation up to hundreds of hours when stored in the dark and measured infrequently. However, these devices rapidly degraded after sustained exposure to sunlight.[10] In addition to light exposure, elevated temperature and humidity may accelerate the degradation due to the moisture-induced decomposition of perovskite crystals.[134] These stability issues, though, are

being addressed by, for example, proper protective coatings. The stability of perovskite PV devices under high humidity and temperature conditions was improved by employing a moisture-resistant layer (e.g., carbon nanotubes or graphite) to prevent water ingress.[93,135–137] Encapsulation techniques using glass sealing or laminate plastic films have also been used to improve device stability to over 3000 h at 60°C under simulated sunlight.[133] Additionally, when incorporating (FA^+ and Br^-) ions into perovskite $(FA_{1-y}MA_y)Pb(I_{3-x}Br_x)$, the thermal and moisture resistivity can be dramatically improved.[32,33,103] These results indicate that perovskite PV modules with appropriate composition and encapsulation have the potential to be stable. It should be noted that good stability of perovskite PV devices has recently been demonstrated under hot outdoor conditions in Jeddah, Saudi Arabia.[137] After three months of operation at 80°C, the perovskite devices demonstrated impressively stable performance without measureable degradation.

6.2 *J – V Hysteresis*

One of the major issues that limits advancement of perovskite solar cells is the presence of the anomalous $J-V$ hysteresis, which is observed by varying the direction and the rate of voltage sweep [Fig. 8(a)].[141] Holding a perovskite device at a forward bias voltage before measurement may result in a higher efficiency than that found when the device is held at the maximum power point or when the device has been reverse biased or held at short circuit.[138] Measuring the device at a rate faster than its response time may also result in varying efficiency measurements.[142] The presence of $J-V$ hysteresis undermines the reporting accuracy of efficiency and may lead to questionable and erroneous device efficiencies.

Parameters affecting $J-V$ hysteresis of perovskite solar cells have been investigated;[143,144] however, the origins of hysteresis remain controversial. Three possible reasons, including ferroelectricity,[145,146] ion migration,[138,140] and unbalanced charge collection rates,[104,147] have been proposed to explain the origin of $J-V$ hysteresis. All of these hypotheses are related to a transient electrical polarization as a response to the change of the external electrical field. Recent

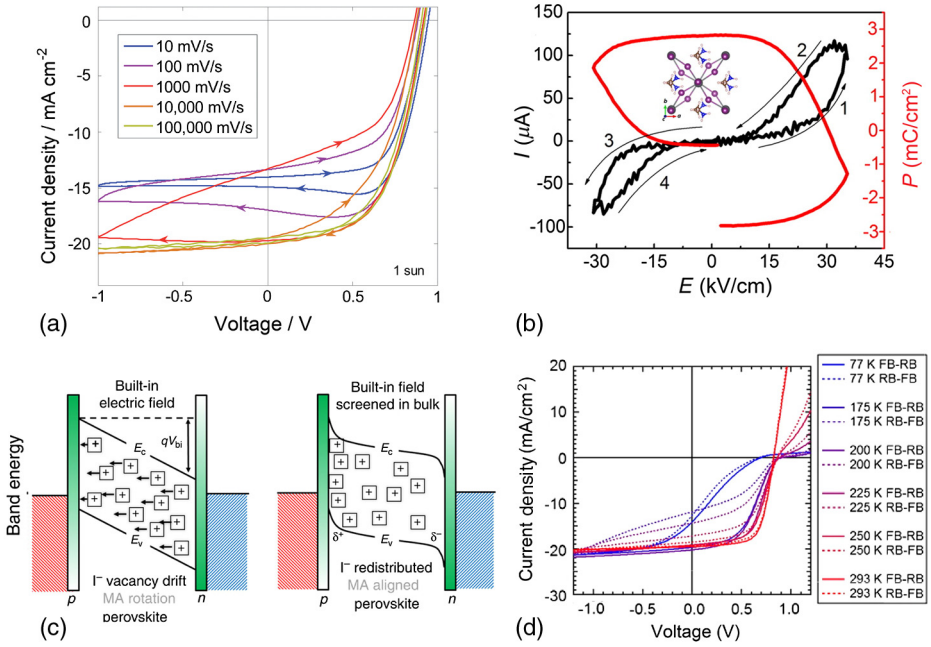

Fig. 8 (a) $J-V$ hysteresis measured using different scan speeds and directions of the scan. Reprinted with permission from Ref. 138. (b) Ferroelectricity of $CH_3NH_3PbI_3$ perovskite. Reprinted with permission from Ref. 139. (c) Schematic diagrams indicating the influence of ion migration in the perovskite solar cells. Reprinted with permission from Ref. 140. (d) Observation of the appearance of substantial $J-V$ hysteresis when cooling the p-i-n perovskite device to 175 K. Reprinted with permission from Ref. 153.

investigations have shown that the latter two are more likely the causes of the $J-V$ hysteresis.[133,148]

Ferroelectricity is one possible but unlikely origin for the $J-V$ hysteresis. Ferroelectricity may occur in OMHPs due to the shift of ions in the crystal away from their corresponding lattice point or the alignment of organic dipole moments. Evidence of this was observed in polarization loops of $MAPbI_3$ thin films and piezoelectric force microscopy.[149,150] However, recent reports indicate that perovskites are not ferroelectric at room temperature [Fig. 8(b)] and that the observed ferroelectric behavior is likely due to piezoelectric or electrochemical behavior.[139,151]

Ion migration is another possible explanation of $J-V$ hysteresis. Under an external electric field, the positive and negative ionic species will migrate to the opposite sides of the device, forming space charge regions closed to the interfaces. Accumulation of the mobile ions changes the density of free electronic charge carries and thus shifts the local quasi-Fermi level in the direction that is favorable (or unfavorable) to charge extraction under positive (or negative) bias [Fig. 8(c)]. Such ion migration has also been demonstrated in polarization-switchable perovskite devices, in which photocurrent direction could be switched by changing the voltage sweep direction.[152] Recent modeling work revealed that the ion migration is accompanied by the charge traps serving as recombination centers.[148] Therefore, reducing the density of mobile ions or charge traps inside the absorber and at the interfaces may alleviate the hysteresis.

Charge transfer rates at the interfaces of the perovskite absorber also strongly influence $J-V$ hysteresis. If unbalanced charge collection exists, i.e., if the charge transfer rates between perovskite and the n-/p-type selective contacts are quite different, charges will accumulate on the interface with a lower charge collection rate and build up a transient capacitance. Evidence of trapped charges was found at two interfaces in the conventional n-i-p structure,[147] where the electron and hole mobilities in the ETM and HTM differ, respectively.[104] Interestingly, the n-i-p device employing a thin mesoporous ETM and an HTM with desired hole mobility typically exhibits negligible hysteresis, which is likely due to the enhanced surface area for electron injection and improved hole transport, respectively. In contrast, the inverted p-i-n cells exhibit much less $J-V$ hysteresis, presumably due to a balanced charge carrier transport and surface passivation on the perovskite/fullerene interface.[104] However, it was demonstrated that the so-called hysteresis-free p-i-n devices exhibit substantial $J-V$ hysteresis when the temperature is reduced to 175 K [Fig. 8(d)].[153] Thus, changing the device architecture may not address the underlying mechanism of hysteresis in the perovskite materials themselves. Moreover, as the devices aged, the $J-V$ hysteresis was aggravated due to the degraded electronic quality of perovskite, especially at interfaces.[138] This shows the importance of improving the stability of the perovskite and the engineering at the interfaces to prevent materials degradation. Furthermore, compositional engineering may also reduce the $J-V$ hysteresis. Unlike $MAPbI_3$, $FAPbI_3$ possesses an asymmetric charge transfer rate, which balances the charge extraction at either side of the perovskite and alleviates the $J-V$ hysteresis.[56] Further development may show that the $J-V$ hysteresis could be reduced or eliminated.

6.3 *Toxicity and Pollution*

Because most perovskite solar cells are lead-based, there are environmental concerns with the possibility of large-scale development. Recent environmental research should reduce these concerns. Ex-ante life cycle analysis and environmental impact assessment of perovskite solar cells have revealed that the lead bears very little proportion on the overall environmental impact during manufacturing process.[154,155] Compared with other lead emission sources, such as mining, fossil fuels, and the manufacture of common products (batteries, plumbing, soldering, electronics, and so on), the potential lead pollution from a 1-GW perovskite PV plant is insignificant, even assuming the worst-case leakage scenario during operation.[156] In fact, perovskite PV may actually be able to reduce the amount of Pb contamination in the environment by providing an opportunity to reuse it from other applications. Recently, perovskite PV devices were fabricated using lead sources recycled from used car batteries.[157] Although no industrial data exist at present, these LCA results are based on the best projections of an industrial process and are likely an overestimate of the potential hazard.

7 Future Directions

A new approach to the design of device architecture for perovskite solar cells is based on the flexible and lightweight substrates (e.g., flexible plastic foils). Such PV devices are of commercial interest for low-cost, large-scale roll-to-roll processing and applications as portable power sources and building/vehicle integrated materials. In the last two years, a great deal of effort has been made on perovskite PV devices on flexible, conductive substrates, such as poly(ethylene terephthalate),[118,158–161] polyethylene naphthalate,[162] and Ti foils.[163] A detailed review of flexible perovskite solar cells can be found elsewhere.[164] The device performances on these substrates were stable after bending.[160,162] Flexible perovskite PV mini-modules have demonstrated the potential to transfer laboratory-based perovskite techniques to industrial roll-to-roll processing[165] and have been used to power aviation models.[166] Additionally, high-transparency and colorful perovskite PV for building integration have also been demonstrated.[167–170]

Because perovskites have a tunable band gap ($E_g = 1.5$ to 2.3 eV) and high V_{OC}, there is great interest in incorporating them in tandem devices with crystal silicon or CIGS cells.[171] It is predicted that the ultimate efficiency of the monolithic tandem perovskite devices can exceed 35% in the future.[11] Several designs of perovskite-based tandem devices have been reported, including two-terminal monolithic devices and four-terminal devices (with a light splitting component).[171–176] However, the overall efficiencies, 19.5% for the best four-terminal perovskite/CIGS device[175] and 21% for the best two-terminal perovskite/Si device,[177] are still lower than that of the state-of-the-art single-junction perovskite devices due to the electric loss at the tunneling junction and the transparent electrode. Practical fabrication of monolithic perovskite tandem devices is challenging because the device efficiency is strongly determined by the choice of the materials and the processing methods. In particular, the tunneling layer needs to be adequately adjusted so that the optical transparency and electrical conductivity can be appropriately matched to both the top and bottom cells. Additionally, the high energy associated with the sputtering of the transparent electrode (ITO or ZnO:Al) may deteriorate the perovskite layer. Therefore, the deposition process needs to be well controlled to prevent any degradation of perovskite or organic HTM layers.

8 Summary

The last five years have witnessed a rapid development of OMHP solar cells. A variety of device architectures and material preparation methods have been developed for fabricating high-performance PV devices. Recent advances in engineering the bulk and interface properties of perovskite thin films and contacts have been tremendously effective in enhancing device performance. These advanced engineering techniques are beneficial to increase perovskite grain size and crystallinity, to improve surface coverage and film morphology, and to passivate surface and bulk defects. Further improvement of perovskite PV devices depends on a precise control of the processing of the organic and inorganic precursors and a corresponding understanding of the fundamental material properties of the perovskites. With progress in device stability, perovskite solar cells may well be a very promising technology for the future PV market.

Acknowledgments

The work was supported by the Air Force Research Laboratory, Space Vehicles Directorate (Contract No. FA9453-11-C-0253) and the National Science Foundation (Contract No. CHE-1230246).

References

1. D. M. Chapin, C. S. Fuller, and G. L. Pearson, "A new silicon p-n junction photocell for converting solar radiation into electrical power," *J. Appl. Phys.* **25**(5), 676–677 (1954).
2. Fraunhofer Institute for Solar Energy Systems, "Photovoltaic report," 2015, https://www.ise.fraunhofer.de/de/downloads/pdf-files/aktuelles/photovoltaics-report-in-englischer-sprache.pdf (29 December 2015).

3. M. A. Green et al., "Solar cell efficiency tables (version 47)," *Prog. Photovolt.* **24**(1), 3–11 (2016).
4. H. J. Snaith, "Perovskites: the emergence of a new era for low-cost, high-efficiency solar cells," *J. Phys. Chem. Lett.* **4**(21), 3623–3630 (2013).
5. N.-G. Park, "Organometal perovskite light absorbers toward a 20% efficiency low-cost solid-state mesoscopic solar cell," *J. Phys. Chem. Lett.* **4**(15), 2423–2429 (2013).
6. R. F. Service, "Perovskite solar cells keep on surging," *Science* **344**(6183), 458 (2014).
7. M. A. Green, A. Ho-Baillie, and H. J. Snaith, "The emergence of perovskite solar cells," *Nat. Photon.* **8**(7), 506–514 (2014).
8. M. Gratzel, "The light and shade of perovskite solar cells," *Nat. Mater.* **13**(9), 838–842 (2014).
9. P. Gao, M. Gratzel, and M. K. Nazeeruddin, "Organohalide lead perovskites for photovoltaic applications," *Energy Environ. Sci.* **7**(8), 2448–2463 (2014).
10. S. D. Stranks and H. J. Snaith, "Metal-halide perovskites for photovoltaic and light-emitting devices," *Nat. Nanotechnol.* **10**(5), 391–402 (2015).
11. Q. Chen et al., "Under the spotlight: the organic-inorganic hybrid halide perovskite for optoelectronic applications," *Nano Today* **10**(3), 355–396 (2015).
12. T. C. Sum and N. Mathews, "Advancements in perovskite solar cells: photophysics behind the photovoltaics," *Energy Environ. Sci.* **7**(8), 2518–2534 (2014).
13. A. K. Chilvery et al., "Perovskites: transforming photovoltaics, a mini-review," *J. Photon. Energy* **5**(1), 057402 (2015).
14. V. S. Sivaram, S. D. Stranks, and H. J. Snaith, "Perovskite solar cells join the major league," *Science* **350**(6263), 917–917 (2015).
15. L. J. Schmidt, "Tracking down the truth of perovski," in *38th Rochester Mineralogical Symp. Program Notes*, pp. 31–32 (2011).
16. M. I. Saidaminov et al., "High-quality bulk hybrid perovskite single crystals within minutes by inverse temperature crystallization," *Nat. Commun.* **6**, 7586 (2015).
17. D. B. Mitzi, "Synthesis, crystal structure, and optical and thermal properties of $(C_4H_9NH_3)_2MI_4$ (M = Ge, Sn, Pb)," *Chem. Mater.* **8**(3), 791–800 (1996).
18. D. B. Mitzi, M. T. Prikas, and K. Chondroudis, "Thin film deposition of organic-inorganic hybrid materials using a single source thermal ablation technique," *Chem. Mater.* **11**(3), 542–544 (1999).
19. D. B. Mitzi, C. D. Dimitrakopoulos, and L. L. Kosbar, "Structurally tailored organic-inorganic perovskites: optical properties and solution-processed channel materials for thin-film transistors," *Chem. Mater.* **13**(10), 3728–3740 (2001).
20. J. Calabrese et al., "Preparation and characterization of layered lead halide compounds," *J. Am. Chem. Soc.* **113**(6), 2328–2330 (1991).
21. K. Chondroudis and D. B. Mitzi, "Electroluminescence from an organic-inorganic perovskite incorporating a quaterthiophene dye within lead halide perovskite layers," *Chem. Mater.* **11**(11), 3028–3030 (1999).
22. D. B. Mitzi, K. Chondroudis, and C. R. Kagan, "Organic-inorganic electronics," *IBM J. Res. Dev.* **45**(1), 29–45 (2001).
23. A. Kojima et al., "Organometal halide perovskites as visible-light sensitizers for photovoltaic cells," *J. Am. Chem. Soc.* **131**(17), 6050–6051 (2009).
24. Editorial, "Perovskite fever," *Nat. Mater.* **13**(9), 837 (2014).
25. H.-S. Kim et al., "Lead iodide perovskite sensitized all-solid-state submicron thin film mesoscopic solar cell with efficiency exceeding 9%," *Sci. Rep.* **2**, 591 (2012).
26. M. M. Lee et al., "Efficient hybrid solar cells based on meso-superstructured organometal halide perovskites," *Science* **338**(6107), 643–647 (2012).
27. NREL, "Solar cell efficiency chart," http://www.nrel.gov/ncpv/images/efficiency_chart.jpg (09 March 2016).
28. J. Burschka et al., "Sequential deposition as a route to high-performance perovskite-sensitized solar cells," *Nature* **499**(7458), 316–319 (2013).
29. M. Liu, M. B. Johnston, and H. J. Snaith, "Efficient planar heterojunction perovskite solar cells by vapour deposition," *Nature* **501**(7467), 395–398 (2013).

30. Q. Chen et al., "Planar heterojunction perovskite solar cells via vapor-assisted solution process," *J. Am. Chem. Soc.* **136**(2), 622–625 (2014).
31. C.-W. Chen et al., "Efficient and uniform planar-type perovskite solar cells by simple sequential vacuum deposition," *Adv. Mater.* **26**(38), 6647–6652 (2014).
32. J. H. Noh et al., "Chemical management for colorful, efficient, and stable inorganic-organic hybrid nanostructured solar cells," *Nano Lett.* **13**(4), 1764–1769 (2013).
33. G. E. Eperon et al., "Formamidinium lead trihalide: a broadly tunable perovskite for efficient planar heterojunction solar cells," *Energy Environ. Sci.* **7**(3), 982–988 (2014).
34. W. J. Yin, T. T. Shi, and Y. F. Yan, "Unique properties of halide perovskites as possible origins of the superior solar cell performance," *Adv. Mater.* **26**(27), 4653–4658 (2014).
35. S. De Wolf et al., "Organometallic halide perovskites: sharp optical absorption edge and its relation to photovoltaic performance," *J. Phys. Chem. Lett.* **5**(6), 1035–1039 (2014).
36. C. S. Ponseca, Jr. et al., "Organometal halide perovskite solar cell materials rationalized: ultrafast charge generation, high and microsecond-long balanced mobilities, and slow recombination," *J. Am. Chem. Soc.* **136**(14), 5189–5192 (2014).
37. V. D'Innocenzo et al., "Excitons versus free charges in organo-lead tri-halide perovskites," *Nat. Commun.* **5**, 3586 (2014).
38. S. D. Stranks et al., "Recombination kinetics in organic-inorganic perovskites: excitons, free charge, and subgap states," *Phys. Rev. Appl.* **2**(3), 034007 (2014).
39. S. D. Stranks et al., "Electron-hole diffusion lengths exceeding 1 micrometer in an organometal trihalide perovskite absorber," *Science* **342**(6156), 341–344 (2013).
40. G. Xing et al., "Long-range balanced electron- and hole-transport lengths in organic-inorganic $CH_3NH_3PbI_3$," *Science* **342**(6156), 344–347 (2013).
41. C. Wehrenfennig et al., "High charge carrier mobilities and lifetimes in organolead trihalide perovskites," *Adv. Mater.* **26**(10), 1584–1589 (2014).
42. T. Leijtens et al., "Electronic properties of meso-superstructured and planar organometal halide perovskite films: charge trapping, photodoping, and carrier mobility," *ACS Nano* **8**(7), 7147–7155 (2014).
43. W.-J. Yin, T. Shi, and Y. Yan, "Unusual defect physics in $CH_3NH_3PbI_3$ perovskite solar cell absorber," *Appl. Phys. Lett.* **104**(6), 063903 (2014).
44. W. Tress et al., "Predicting the open-circuit voltage of $CH_3NH_3PbI_3$ perovskite solar cells using electroluminescence and photovoltaic quantum efficiency spectra: the role of radiative and non-radiative recombination," *Adv. Energy Mater.* **5**(3), 1400812 (2015).
45. J. H. Im et al., "6.5% efficient perovskite quantum-dot-sensitized solar cell," *Nanoscale* **3**(10), 4088–4093 (2011).
46. B. O'Regan and M. Gratzel, "A low-cost, high-efficiency solar cell based on dye-sensitized colloidal TiO_2 films," *Nature* **353**(6346), 737–740 (1991).
47. W. Chen et al., "Hybrid interfacial layer leads to solid performance improvement of inverted perovskite solar cells," *Energy Environ. Sci.* **8**(2), 629–640 (2015).
48. K. C. Wang et al., "P-type mesoscopic nickel oxide/organometallic perovskite heterojunction solar cells," *Sci. Rep.* **4**, 4756 (2014).
49. M. Lee et al., "Efficient, durable and flexible perovskite photovoltaic devices with Ag-embedded ITO as the top electrode on a metal substrate," *J. Mater. Chem. A* **3**(28), 14592–14597 (2015).
50. J. Troughton et al., "Highly efficient, flexible, indium-free perovskite solar cells employing metallic substrates," *J. Mater. Chem. A* **3**(17), 9141–9145 (2015).
51. J. H. Heo et al., "Efficient inorganic-organic hybrid heterojunction solar cells containing perovskite compound and polymeric hole conductors," *Nat. Photon.* **7**(6), 486–491 (2013).
52. J. J. Choi et al., "Structure of methylammonium lead iodide within mesoporous titanium dioxide: active material in high-performance perovskite solar cells," *Nano Lett.* **14**(1), 127–133 (2014).
53. T. Leijtens et al., "Overcoming ultraviolet light instability of sensitized TiO_2 with meso-superstructured organometal tri-halide perovskite solar cells," *Nat. Commun.* **4**, 2885 (2013).
54. T. Leijtens et al., "The importance of perovskite pore filling in organometal mixed halide sensitized TiO_2-based solar cells," *J. Phys. Chem. Lett.* **5**(7), 1096–1102 (2014).

55. G. E. Eperon et al., "Morphological control for high performance, solution-processed planar heterojunction perovskite solar cells," *Adv. Funct. Mater.* **24**(1), 151–157 (2014).
56. W. S. Yang et al., "High-performance photovoltaic perovskite layers fabricated through intramolecular exchange," *Science* **348**(6240), 1234–1237 (2015).
57. E. Edri et al., "Why lead methylammonium tri-iodide perovskite-based solar cells require a mesoporous electron transporting scaffold (but not necessarily a hole conductor)," *Nano Lett.* **14**(2), 1000–1004 (2014).
58. H. Zhou et al., "Interface engineering of highly efficient perovskite solar cells," *Science* **345**(6196), 542–546 (2014).
59. J.-Y. Jeng et al., "$CH_3NH_3PbI_3$ perovskite/fullerene planar-heterojunction hybrid solar cells," *Adv. Mater.* **25**(27), 3727–3732 (2013).
60. O. Malinkiewicz et al., "Perovskite solar cells employing organic charge-transport layers," *Nat. Photon.* **8**(2), 128–132 (2014).
61. Q. Dong et al., "Abnormal crystal growth in $CH_3NH_3PbI_{3-x}CL_x$ using a multi-cycle solution coating process," *Energy Environ. Sci.* **8**(8), 2464–2470 (2015).
62. W. Chen et al., "Efficient and stable large-area perovskite solar cells with inorganic charge extraction layers," *Science* **350**(6263), 944–948 (2015).
63. J. You et al., "Improved air stability of perovskite solar cells via solution-processed metal oxide transport layers," *Nat. Nanotechnol.* **11**(1), 75–81 (2016).
64. J. H. Park et al., "Efficient $CH_3NH_3PbI_3$ perovskite solar cells employing nanostructured p-type nio electrode formed by a pulsed laser deposition," *Adv. Mater.* **27**(27), 4013–4019 (2015).
65. Z. Song et al., "Impact of processing temperature and composition on the formation of methylammonium lead iodide perovskites," *Chem. Mater.* **27**(13), 4612–4619 (2015).
66. C. Roldan-Carmona et al., "High efficiency methylammonium lead triiodide perovskite solar cells: the relevance of non-stoichiometric precursors," *Energy Environ. Sci.* **8**(12), 3550–3556 (2015).
67. Q. Wang et al., "Large fill-factor bilayer iodine perovskite solar cells fabricated by a low-temperature solution-process," *Energy Environ. Sci.* **7**(7), 2359–2365 (2014).
68. J.-H. Im et al., "Growth of $CH_3NH_3PbI_3$ cuboids with controlled size for high-efficiency perovskite solar cells," *Nat. Nanotechnol.* **9**(11), 927–932 (2014).
69. N. Ahn et al., "Highly reproducible perovskite solar cells with average efficiency of 18.3% and best efficiency of 19.7% fabricated via Lewis base adduct of lead(II) iodide," *J. Am. Chem. Soc.* **137**(27), 8696–8699 (2015).
70. A. T. Barrows et al., "Efficient planar heterojunction mixed-halide perovskite solar cells deposited via spray-deposition," *Energy Environ. Sci.* **7**(9), 2944–2950 (2014).
71. Y. H. Deng et al., "Scalable fabrication of efficient organolead trihalide perovskite solar cells with doctor-bladed active layers," *Energy Environ. Sci.* **8**(5), 1544–1550 (2015).
72. S.-G. Li et al., "Inkjet printing of $CH_3NH_3PbI_3$ on a mesoscopic TiO_2 film for highly efficient perovskite solar cells," *J. Mater. Chem. A* **3**(17), 9092–9097 (2015).
73. K. Hwang et al., "Toward large scale roll-to-roll production of fully printed perovskite solar cells," *Adv. Mater.* **27**(7), 1241–1247 (2015).
74. K. N. Liang, D. B. Mitzi, and M. T. Prikas, "Synthesis and characterization of organic-inorganic perovskite thin films prepared using a versatile two-step dipping technique," *Chem. Mater.* **10**(1), 403–411 (1998).
75. Z. Song et al., "Spatially resolved characterization of solution processed perovskite solar cells using the lbic technique," in *IEEE 42nd Photovoltaic Specialist Conf.*, pp. 1–5 (2015).
76. T. Zhang et al., "Controllable sequential deposition of planar $CH_3NH_3PbI_3$ perovskite films via adjustable volume expansion," *Nano Lett.* **15**(6), 3959–3963 (2015).
77. N. J. Jeon et al., "Solvent engineering for high-performance inorganic-organic hybrid perovskite solar cells," *Nat. Mater.* **13**(9), 897–903 (2014).
78. V. Nicolosi et al., "Liquid exfoliation of layered materials," *Science* **340**(6139), 1226419 (2013).
79. F. Hao et al., "Controllable perovskite crystallization at a gas-solid interface for hole conductor-free solar cells with steady power conversion efficiency over 10%," *J. Am. Chem. Soc.* **136**(46), 16411–16419 (2014).

80. M. M. Tavakoli et al., "Fabrication of efficient planar perovskite solar cells using a one-step chemical vapor deposition method," *Sci. Rep.* **5**, 14083 (2015).
81. Q. Lin et al., "Electro-optics of perovskite solar cells," *Nat. Photon.* **9**(2), 106–112 (2015).
82. D. Zhao et al., "Annealing-free efficient vacuum-deposited planar perovskite solar cells with evaporated fullerenes as electron-selective layers," *Nano Energy* **19**, 88–97 (2016).
83. T. Salim et al., "Perovskite-based solar cells: impact of morphology and device architecture on device performance," *J. Mater. Chem. A* **3**(17), 8943–8969 (2015).
84. Y. Zhao and K. Zhu, "Solution chemistry engineering toward high-efficiency perovskite solar cells," *J. Phys. Chem. Lett.* **5**(23), 4175–4186 (2014).
85. K. Yan et al., "Hybrid halide perovskite solar cell precursors: colloidal chemistry and coordination engineering behind device processing for high efficiency," *J. Am. Chem. Soc.* **137**(13), 4460–4468 (2015).
86. W. Li et al., "Controllable grain morphology of perovskite absorber film by molecular self-assembly toward efficient solar cell exceeding 17%," *J. Am. Chem. Soc.* **137**(32), 10399–10405 (2015).
87. Y. Zhao and K. Zhu, "Efficient planar perovskite solar cells based on 1.8 eV band gap $CH_3NH_3PbI_32Br$ nanosheets via thermal decomposition," *J. Am. Chem. Soc.* **136**(35), 12241–12244 (2014).
88. J. H. Heo et al., "Planar $CH_3NH_3PbI_3$ perovskite solar cells with constant 17.2% average power conversion efficiency irrespective of the scan rate," *Adv. Mater.* **27**(22), 3424–3430 (2015).
89. H. Tsai et al., "Optimizing composition and morphology for large-grain perovskite solar cells via chemical control," *Chem. Mater.* **27**(16), 5570–5576 (2015).
90. Y. Chen, Y. Zhao, and Z. Liang, "Non-thermal annealing fabrication of efficient planar perovskite solar cells with inclusion of NH_4Cl," *Chem. Mater.* **27**(5), 1448–1451 (2015).
91. J. H. Heo, D. H. Song, and S. H. Im, "Planar $CH_3NH_3PbBr_3$ hybrid solar cells with 10.4% power conversion efficiency, fabricated by controlled crystallization in the spin-coating process," *Adv. Mater.* **26**(48), 8179–8183 (2014).
92. P. W. Liang et al., "Additive enhanced crystallization of solution-processed perovskite for highly efficient planar-heterojunction solar cells," *Adv. Mater.* **26**(22), 3748–3754 (2014).
93. A. Mei et al., "A hole-conductor-free, fully printable mesoscopic perovskite solar cell with high stability," *Science* **345**(6194), 295–298 (2014).
94. X. Li et al., "Improved performance and stability of perovskite solar cells by crystal cross-linking with alkylphosphonic acid ω-ammonium chlorides," *Nat. Chem.* **7**(9), 703–711 (2015).
95. Y. Wu et al., "Retarding the crystallization of PbI_2 for highly reproducible planar-structured perovskite solar cells via sequential deposition," *Energy Environ. Sci.* **7**(9), 2934–2938 (2014).
96. C. G. Wu et al., "High efficiency stable inverted perovskite solar cells without current hysteresis," *Energy Environ. Sci.* **8**(9), 2725–2733 (2015).
97. W. Nie et al., "High-efficiency solution-processed perovskite solar cells with millimeter-scale grains," *Science* **347**(6221), 522–525 (2015).
98. Y. C. Zheng et al., "Thermal-induced Volmer-Weber growth behavior for planar heterojunction perovskites solar cells," *Chem. Mater.* **27**(14), 5116–5121 (2015).
99. M. Xiao et al., "A fast deposition-crystallization procedure for highly efficient lead iodide perovskite thin-film solar cells," *Angew. Chem.* **53**(37), 9898–9903 (2014).
100. Z. Xiao et al., "Solvent annealing of perovskite-induced crystal growth for photovoltaic-device efficiency enhancement," *Adv. Mater.* **26**(37), 6503–6509 (2014).
101. D. W. de Quilettes et al., "Impact of microstructure on local carrier lifetime in perovskite solar cells," *Science* **348**(6235), 683–686 (2015).
102. B. S. Tosun and H. W. Hillhouse, "Enhanced carrier lifetimes of pure iodide hybrid perovskite via vapor-equilibrated re-growth (VERG)," *J. Phys. Chem. Lett.* **6**(13), 2503–2508 (2015).
103. N. J. Jeon et al., "Compositional engineering of perovskite materials for high-performance solar cells," *Nature* **517**(7535), 476–480 (2015).
104. J. H. Heo et al., "Hysteresis-less inverted $CH_3NH_3PbI_3$ planar perovskite hybrid solar cells with 18.1% power conversion efficiency," *Energy Environ. Sci.* **8**(5), 1602–1608 (2015).

105. J. P. Correa Baena et al., "Highly efficient planar perovskite solar cells through band alignment engineering," *Energy Environ. Sci.* **8**(10), 2928–2934 (2015).
106. H. D. Kim et al., "Photovoltaic performance of perovskite solar cells with different grain sizes," *Adv. Mater.* **28**(5), 917–922 (2016).
107. J. W. Jung, C.-C. Chueh, and A. K. Y. Jen, "A low-temperature, solution-processable, Eu-doped nickel oxide hole-transporting layer via the combustion method for high-performance thin-film perovskite solar cells," *Adv. Mater.* **27**(47), 7874–7880 (2015).
108. N. Pellet et al., "Mixed-organic-cation perovskite photovoltaics for enhanced solar-light harvesting," *Angew. Chem.* **53**(12), 3151–3157 (2014).
109. N. K. Noel et al., "Lead-free organic-inorganic tin halide perovskites for photovoltaic applications," *Energy Environ. Sci.* **7**(9), 3061–3068 (2014).
110. F. Hao et al., "Lead-free solid-state organic-inorganic halide perovskite solar cells," *Nat. Photon.* **8**(6), 489–494 (2014).
111. Y. Ogomi et al., "$CH_3NH_3Sn_xPb_{(1-x)}I_3$ perovskite solar cells covering up to 1060 nm," *J. Phys. Chem. Lett.* **5**(6), 1004–1011 (2014).
112. F. Hao et al., "Solvent-mediated crystallization of $CH_3NH_3SnI_3$ films for heterojunction depleted perovskite solar cells," *J. Am. Chem. Soc.* **137**(35), 11445–11452 (2015).
113. H. S. Kim et al., "Mechanism of carrier accumulation in perovskite thin-absorber solar cells," *Nat. Commun.* **4**, 7 (2013).
114. D. Y. Son et al., "11% efficient perovskite solar cell based on Zno nanorods: an effective charge collection system," *J. Phys. Chem. C* **118**(30), 16567–16573 (2014).
115. J. M. Ball et al., "Low-temperature processed meso-superstructured to thin-film perovskite solar cells," *Energy Environ. Sci.* **6**(6), 1739–1743 (2013).
116. A. Bera et al., "Perovskite oxide $SrTiO_3$ as an efficient electron transporter for hybrid perovskite solar cells," *J. Phys. Chem. C* **118**(49), 28494–28501 (2014).
117. D. Q. Bi et al., "Using a two-step deposition technique to prepare perovskite ($CH_3NH_3PbI_3$) for thin film solar cells based on ZrO_2 and TiO_2 mesostructures," *RSC Adv.* **3**(41), 18762–18766 (2013).
118. D. Liu and T. L. Kelly, "Perovskite solar cells with a planar heterojunction structure prepared using room-temperature solution processing techniques," *Nat. Photon.* **8**(2), 133–138 (2014).
119. W. Ke et al., "Low-temperature solution-processed tin oxide as an alternative electron transporting layer for efficient perovskite solar cells," *J. Am. Chem. Soc.* **137**(21), 6730–6733 (2015).
120. L. Wang et al., "Low temperature solution processed planar heterojunction perovskite solar cells with a CDSE nanocrystal as an electron transport/extraction layer," *J. Mater. Chem. C* **2**(43), 9087–9090 (2014).
121. J. Liu et al., "Low-temperature, solution processed metal sulfide as an electron transport layer for efficient planar perovskite solar cells," *J. Mater. Chem. A* **3**(22), 11750–11755 (2015).
122. J. T. W. Wang et al., "Low-temperature processed electron collection layers of graphene/TiO_2 nanocomposites in thin film perovskite solar cells," *Nano Lett.* **14**(2), 724–730 (2014).
123. Z. Yu and L. Sun, "Recent progress on hole-transporting materials for emerging organometal halide perovskite solar cells," *Adv. Energy Mater.* **5**(12), 1500213 (2015).
124. P. Qin et al., "Inorganic hole conductor-based lead halide perovskite solar cells with 12.4% conversion efficiency," *Nat. Commun.* **5**, 3834 (2014).
125. S. Ye et al., "CuSCN-based inverted planar perovskite solar cell with an average PCE of 15.6%," *Nano Lett.* **15**(6), 3723–3728 (2015).
126. J. A. Christians, R. C. M. Fung, and P. V. Kamat, "An inorganic hole conductor for organo-lead halide perovskite solar cells. Improved hole conductivity with copper iodide," *J. Am. Chem. Soc.* **136**(2), 758–764 (2014).
127. X. Xu et al., "Hole selective NiO contact for efficient perovskite solar cells with carbon electrode," *Nano Lett.* **15**(4), 2402–2408 (2015).
128. L. Etgar et al., "Mesoscopic $CH_3NH_3PbI_3/TiO_2$ heterojunction solar cells," *J. Am. Chem. Soc.* **134**(42), 17396–17399 (2012).

129. W. A. Laban and L. Etgar, "Depleted hole conductor-free lead halide iodide heterojunction solar cells," *Energy Environ. Sci.* **6**(11), 3249–3253 (2013).
130. J. Shi et al., "Hole-conductor-free perovskite organic lead iodide heterojunction thin-film solar cells: high efficiency and junction property," *Appl. Phys. Lett.* **104**(6), 063901 (2014).
131. W. Ke et al., "Efficient hole-blocking layer-free planar halide perovskite thin-film solar cells," *Nat. Commun.* **6**, 6700 (2015).
132. D. Liu, J. Yang, and T. L. Kelly, "Compact layer free perovskite solar cells with 13.5% efficiency," *J. Am. Chem. Soc.* **136**(49), 17116–17122 (2014).
133. T. Leijtens et al., "Stability of metal halide perovskite solar cells," *Adv. Energy Mater.* **5**, 1500963 (2015).
134. J. M. Frost et al., "Atomistic origins of high-performance in hybrid halide perovskite solar cells," *Nano Lett.* **14**(5), 2584–2590 (2014).
135. S. N. Habisreutinger et al., "Carbon nanotube/polymer composites as a highly stable hole collection layer in perovskite solar cells," *Nano Lett.* **14**(10), 5561–5568 (2014).
136. Z. Song et al., "Investigation of degradation mechanisms of perovskite-based photovoltaic devices using laser beam induced current mapping," *Proc. SPIE* **9561**, 956107 (2015).
137. X. Li et al., "Outdoor performance and stability under elevated temperatures and long-term light soaking of triple-layer mesoporous perovskite photovoltaics," *Energy Technol.* **3**(6), 551–555 (2015).
138. W. Tress et al., "Understanding the rate-dependent J-V hysteresis, slow time component, and aging in $CH_3NH_3PbI_3$ perovskite solar cells: the role of a compensated electric field," *Energy Environ. Sci.* **8**(3), 995–1004 (2015).
139. Z. Fan et al., "Ferroelectricity of $CH_3NH_3PbI_3$ perovskite," *J. Phys. Chem. Lett.* **6**(7), 1155–1161 (2015).
140. C. Eames et al., "Ionic transport in hybrid lead iodide perovskite solar cells," *Nat. Commun.* **6**, 7497 (2015).
141. H. J. Snaith et al., "Anomalous hysteresis in perovskite solar cells," *J. Phys. Chem. Lett.* **5**(9), 1511–1515 (2014).
142. E. L. Unger et al., "Hysteresis and transient behavior in current-voltage measurements of hybrid-perovskite absorber solar cells," *Energy Environ. Sci.* **7**(11), 3690–3698 (2014).
143. H.-S. Kim and N.-G. Park, "Parameters affecting I-V hysteresis of $CH_3NH_3PbI_3$ perovskite solar cells: effects of perovskite crystal size and mesoporous TiO_2 layer," *J. Phys. Chem. Lett.* **5**(17), 2927–2934 (2014).
144. Y. Shao et al., "Origin and elimination of photocurrent hysteresis by fullerene passivation in $CH_3NH_3PbI_3$ planar heterojunction solar cells," *Nat. Commun.* **5**, 5784 (2014).
145. J. Wei et al., "Hysteresis analysis based on the ferroelectric effect in hybrid perovskite solar cells," *J. Phys. Chem. Lett.* **5**(21), 3937–3945 (2014).
146. J. M. Frost, K. T. Butler, and A. Walsh, "Molecular ferroelectric contributions to anomalous hysteresis in hybrid perovskite solar cells," *APL Mater.* **2**(8), 081506 (2014).
147. V. W. Bergmann et al., "Real-space observation of unbalanced charge distribution inside a perovskite-sensitized solar cell," *Nat. Commun.* **5**, 5001 (2014).
148. S. van Reenen, M. Kemerink, and H. J. Snaith, "Modeling anomalous hysteresis in perovskite solar cells," *J. Phys. Chem. Lett.* **6**(19), 3808–3814 (2015).
149. J. Beilsten-Edmands et al., "Non-ferroelectric nature of the conductance hysteresis in $CH_3NH_3PbI_3$ perovskite-based photovoltaic devices," *Appl. Phys. Lett.* **106**(17), 173502 (2015).
150. B. Chen et al., "Ferroelectric solar cells based on inorganic-organic hybrid perovskites," *J. Mater. Chem. A* **3**(15), 7699–7705 (2015).
151. M. Coll et al., "Polarization switching and light-enhanced piezoelectricity in lead halide perovskites," *J. Phys. Chem. Lett.* **6**(8), 1408–1413 (2015).
152. Z. Xiao et al., "Giant switchable photovoltaic effect in organometal trihalide perovskite devices," *Nat. Mater.* **14**(2), 193–198 (2015).
153. D. Bryant et al., "Observable hysteresis at low temperature in 'hysteresis free' organic-inorganic lead halide perovskite solar cells," *J. Phys. Chem. Lett.* **6**(16), 3190–3194 (2015).

154. J. Gong, S. B. Darling, and F. You, "Perovskite photovoltaics: life-cycle assessment of energy and environmental impacts," *Energy Environ. Sci.* **8**(7), 1953–1968 (2015).
155. N. Espinosa et al., "Solution and vapour deposited lead perovskite solar cells: ecotoxicity from a life cycle assessment perspective," *Sol. Energy Mater. Sol. Cells* **137**, 303–310 (2015).
156. B. Hailegnaw et al., "Rain on methylammonium lead iodide based perovskites: possible environmental effects of perovskite solar cells," *J. Phys. Chem. Lett.* **6**(9), 1543–1547 (2015).
157. P. Y. Chen et al., "Environmentally responsible fabrication of efficient perovskite solar cells from recycled car batteries," *Energy Environ. Sci.* **7**(11), 3659–3665 (2014).
158. J. You et al., "Low-temperature solution-processed perovskite solar cells with high efficiency and flexibility," *ACS Nano* **8**(2), 1674–1680 (2014).
159. P. Docampo et al., "Efficient organometal trihalide perovskite planar-heterojunction solar cells on flexible polymer substrates," *Nat. Commun.* **4**, 2761 (2013).
160. C. Roldan-Carmona et al., "Flexible high efficiency perovskite solar cells," *Energy Environ. Sci.* **7**(3), 994–997 (2014).
161. D. Bryant et al., "A transparent conductive adhesive laminate electrode for high-efficiency organic-inorganic lead halide perovskite solar cells," *Adv. Mater.* **26**(44), 7499–7504 (2014).
162. B. J. Kim et al., "Highly efficient and bending durable perovskite solar cells: toward a wearable power source," *Energy Environ. Sci.* **8**(3), 916–921 (2015).
163. X. Y. Wang et al., "TiO_2 nanotube arrays based flexible perovskite solar cells with transparent carbon nanotube electrode," *Nano Energy* **11**, 728–735 (2015).
164. Y. Wang et al., "High-efficiency flexible solar cells based on organometal halide perovskites," *Adv. Mater.* (2015).
165. F. Di Giacomo et al., "Flexible perovskite photovoltaic modules and solar cells based on atomic layer deposited compact layers and uv-irradiated TiO_2 scaffolds on plastic substrates," *Adv. Energy Mater.* **5**(8), 1401808 (2015).
166. M. Kaltenbrunner et al., "Flexible high power-per-weight perovskite solar cells with chromium oxide-metal contacts for improved stability in air," *Nat. Mater.* **14**(10), 1032–1039 (2015).
167. G. E. Eperon et al., "Neutral color semitransparent microstructured perovskite solar cells," *ACS Nano* **8**(1), 591–598 (2014).
168. E. Della Gaspera et al., "Ultra-thin high efficiency semitransparent perovskite solar cells," *Nano Energy* **13**, 249–257 (2015).
169. A. Cannavale et al., "Perovskite photovoltachromic cells for building integration," *Energy Environ. Sci.* **8**(5), 1578–1584 (2015).
170. W. Zhang et al., "Highly efficient perovskite solar cells with tunable structural color," *Nano Lett.* **15**(3), 1698–1702 (2015).
171. C. D. Bailie et al., "Semi-transparent perovskite solar cells for tandems with silicon and CIGS," *Energy Environ. Sci.* **8**(3), 956–963 (2015).
172. P. Loper et al., "Organic-inorganic halide perovskite/crystalline silicon four-terminal tandem solar cells," *Phys. Chem. Chem. Phys.* **17**(3), 1619–1629 (2015).
173. C. C. Chen et al., "Perovskite/polymer monolithic hybrid tandem solar cells utilizing a low-temperature, full solution process," *Mater. Horiz.* **2**(2), 203–211 (2015).
174. J. P. Mailoa et al., "A 2-terminal perovskite/silicon multijunction solar cell enabled by a silicon tunnel junction," *Appl. Phys. Lett.* **106**(12), 121105 (2015).
175. L. Kranz et al., "High-efficiency polycrystalline thin film tandem solar cells," *J. Phys. Chem. Lett.* **6**(14), 2676–2681 (2015).
176. S. Albrecht et al., "Monolithic perovskite/silicon-heterojunction tandem solar cells processed at low temperature," *Energy Environ. Sci.* **9**, 81–88 (2016).
177. J. Werner et al., "Efficient monolithic perovskite/silicon tandem solar cell with cell area >1 cm^2," *J. Phys. Chem. Lett.* **7**(1), 161–166 (2016).

Zhaoning Song received his BS degree in physics from Xiamen University, China, in 2009. He is currently a PhD student in Dr. Michael Heben's group at the University of Toledo. His research

interests include solution processing of thin-film photovoltaics and nanomaterials for optoelectronic applications. The goal of his research is to develop more cost-effective alternatives to conventional PV technologies and to explore underlying physical processes of preparing the materials.

Suneth C. Watthage is a PhD candidate in the Department of Physics of the University of Toledo in the concentration of material science. He received his BS degree in engineering physics from the University of Colombo, Sri Lanka, in 2008 and his MS degree in engineering technology from Middle Tennessee State University in 2012. His research interests mainly focus on fabrication and characterization of nanomaterials for thin film photovoltaics and opto-electronic devices.

Adam B. Phillips received his BS degree in physics from Case Western Reserve University in 1999 and his PhD in physics from the University of Virginia in 2007. He joined the University of Toledo in 2008 and is currently a research associate professor at UT's Wright Center for Photovoltaic Innovation and Commercialization. His research includes investigating low cost materials and methods for carbon-free energy sources.

Michael J. Heben is a professor and the Wright Center Endowed chair for Photovoltaics in the Department of Physics and Astronomy at the University of Toledo (UT). He earned his MS degree in materials science and engineering from Stanford and his PhD in chemistry from Caltech under the guidance of N.S. Lewis. He became a postdoc with A.J. Nozik at SERI/NREL in 1990, and was a principal scientist and group leader when he left NREL for UT in 2008.